# Experimental Validation of a Unified and Linear State Estimation Method for Hybrid AC/DC Microgrids

Willem Lambrichts, Mario Paolone
Distributed Electrical Systems Laboratory, EPFL, Switzerland
willem.lambrichts@epfl.ch, mario.paolone@epfl.ch

***Abstract*—This paper presents the experimental validation of a linear recursive state estimation (SE) process for hybrid AC/DC microgrids proposed in the authors' previous work. The SE uses a unified and linear measurement model that relies on the use of synchronized AC and DC measurements along with the complex modulation index of voltage source converters (VSCs). The validation is performed on the hybrid AC/DC microgrid available at the EPFL. The hybrid network consists of 18 AC nodes, 8 DC nodes and 4 VSCs interfacing the AC and DC parts of the grid at different nodes. The experimental validation of the measurement model is based on the classical noise model verification via the measurement residuals. It is shown that the measurement residuals of the AC system, DC system and VSC model are zero-biased with a standard deviation well below the three-sigma threshold of the expected noise distribution. An estimation of the prediction error covariance is also implemented and analyzed to automatically adopt the accuracy of the SE during dynamic and steady-state conditions. Furthermore, the time latency of each section in the SE process is analysed to validate its applicability in critical real-time applications.**

***Index Terms*—State estimation, Hybrid AC/DC networks, Experimental validation**

## I. Introduction

Hybrid AC/DC microgrids are a promising solution for future power grids that are expected to heavily rely on renewable sources. Indeed, combining AC with DC systems creates several benefits, such as a higher overall system efficiency [1], a more flexible control (due to the presence of controllable interfacing AC/DC converters) and a reduced system cost because less power converting sources are required as DC sources and loads are directly connected to the DC grid [2]. Different core functionalities of electrical networks require the knowledge of the systems state e.g. security assessment, optimal grid-aware controls and stability analysis [3]. Therefore, state estimation (SE), i.e. the process of computing the most likelihood state of the system using a noisy and incomplete set of measurements, is a critical element in the operation of modern power transmission and distribution systems.

This paper presents the experimental validation of a unified SE model for hybrid AC/DC microgrids that has been proposed in the authors' previous work [4]. The measurement model, linking the states and measurements, is fully linear and includes the AC system's model, DC model and AC/DC converters' interlinking equations that are based on the complex modulation index.

The project has received funding from the European Unions Horizon 2020 Research & Innovation Programme under grant agreement No. 957788.

The validation of the SE model is performed on the hybrid AC/DC network developed at the EPFL. The SE model has been implemented in the Supervisory Control and Data Acquisition (SCADA) system that has been presented in [5]. The SCADA system consists of a data acquisition stage from phasor measurement units (PMU) and time-synchronized DC measurement units (DMUs), a phasor data concentrator (PDC) and the SE. The data acquisition by PMUs and DMUs is characterised by high streaming rates (i.e., in the order of tens of frames per second) that allow for real-time SE with a low latency and a high refresh rate. To the best of the authors' knowledge, this is the first linear SE for hybrid AC/DC networks that has been experimentally validated on a real-world hybrid microgrid.

SE methods proposed in the literature for hybrid AC/DC systems rely mainly on decomposing the problem by solving the AC and DC network equations separately and linking them through an iterative process [6]–[8]. References [9], [10] propose a unified model that includes the power balance equation of the interlinking converter. However, these iterative methods are computationally inefficient and no unique solution can be guaranteed, thus justifying the development of the adopted SE model.

The paper is structured into four sections. Section II describes the adopted linear and unified measurement model for the recursive SE of hybrid AC/DC microgrid proposed in [4]. Furthermore, the complex modulation index and the SE prediction error covariance estimation are recalled. Section III describes the experimental setup. Section IV shows the results of the experimental validation of the SE method and presents a time latency analysis of the individual stages of the SE process. The conclusions are given in Section V.

## II. Summary of the adopted SE method

### A. The recursive state estimator

A recursive SE, and more specifically a discrete Kalman filter (DKF), is used for the SE process. The choice of a DKF relies on the nature of the measurement model that is introduced in subsection II-B. Indeed, the previously estimated state is needed to compute the equivalent series resistance used

to model the losses in the interfacing AC/DC voltage source converters (VSCs) and thus making the SE problem inherently recursive. As known, the DKF relies on a measurement model (1) and a process model (2) to compute the state using the set of $m$-measurements $\mathbf{z} \in \mathbb{R}^m$ [11].

$$\mathbf{z}_k = \mathbf{H}\mathbf{x}_k + \mathbf{v_k}, \quad p(\mathbf{v_k}) \sim \mathcal{N}(0, \mathbf{R}) \tag{1}$$

$$\mathbf{x}_k = \mathbf{x}_{k-1} + \mathbf{w}_{k-1}, \quad p(\mathbf{w}_{k-1}) \sim \mathcal{N}(0, \mathbf{Q}) \tag{2}$$

where $k$ is the discrete time index, $\mathbf{x}_k \in \mathbb{R}^n$ is the estimated state and $\mathbf{H}_k$ the measurement model. The measurement noise $\mathbf{v_k} \in \mathbb{R}^m$ is assumed to be uncorrelated, unbiased and characterized by a white Gaussian covariance matrix $\mathbf{R}$. The noise level associated with each measurement is dependent on the measurement transformers and the PMUs and DMUs accuracy classes as discussed in Section III. The process model accounts for the time evolution of the system states and an ARIMA $(0, 1, 0)$ model [12] is used since is very suitable for the measurements high frame rate in this application where the state between two consecutive timesteps does not change significantly[1]. The process noise follows the same assumptions and has as covariance matrix $\mathbf{Q}$. The DKF consists of a prediction and estimation step:

*Prediction step*:

$$\tilde{\mathbf{x}}_k = \hat{\mathbf{x}}_{k-1} \tag{3}$$

$$\tilde{\mathbf{P}}_k = \hat{\mathbf{P}}_{k-1} + \mathbf{Q}_{k-1} \tag{4}$$

*Estimation step*:

$$\mathbf{K}_k = \tilde{\mathbf{P}}_k \mathbf{H}^T (\mathbf{H}\tilde{\mathbf{P}}_k \mathbf{H}^T + \mathbf{R}_k)^{-1} \tag{5}$$

$$\hat{\mathbf{x}}_k = \tilde{\mathbf{x}}_k + \mathbf{K}_k(\mathbf{z}_k - \mathbf{H}\tilde{\mathbf{x}}_\mathbf{k}) \tag{6}$$

$$\hat{\mathbf{P}}_k = (\mathbf{I} - \mathbf{K}_k\mathbf{H})\tilde{\mathbf{P}}_k, \tag{7}$$

where $\tilde{\mathbf{x}}_\mathbf{k}$ is the process-model predicted state and $\tilde{\mathbf{P}}_k$ and $\hat{\mathbf{P}}_k$ are the prediction error and estimation error covariance matrices.

### B. Measurement model

The measurement model (1) for hybrid AC/DC SE gives a linear relationship between the measurements $\mathbf{z} = [\mathbf{z}_{ac}\ \mathbf{z}_{dc}\ \mathbf{z}_{vsc}]^\intercal$ and the states $\mathbf{x} = [\mathbf{x}_{ac}\ \mathbf{x}_{dc}]^\intercal$ [4]. The states of a power system are typically the nodal voltage phasors and the measurements are nodal voltages, current injections and flows. The consequent measurement model matrix $\mathbf{H}$ has the following form:

$$\mathbf{H} = \begin{bmatrix} \mathbf{H}_{ac-ac} & \mathbf{0} \\ \mathbf{0} & \mathbf{H}_{dc-dc} \\ \mathbf{H}_{vsc-ac} & \mathbf{H}_{vsc-dc} \end{bmatrix} \tag{8}$$

The submatrix $\mathbf{H}_{ac-ac}$ is the measurement model for the AC system and is strictly linear when written in Cartesian coordinates with PMUs providing synchronised voltage and current measurements [11]. The submatrix $\mathbf{H}_{dc-dc}$ links the DC measurements coming from the DMUs to the DC states in an intrinsically linear way. The remaining submatrices

[1]In the case this is not true, the SE process suitably adapts the process model covariance $\mathbf{Q}$ (see Section II-D)

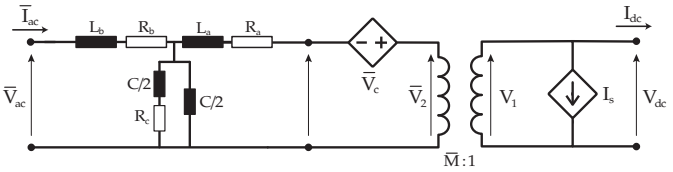


**Fig. 1:** Transformer-like model of an inverter leg of the AC/DC converter with LCL filter and losses

represent the VSC model linking its measurements to the AC and DC states. Details on the composition of the measurement matrix are given in Section III. The measurement model is introduced in [4] and is based on the complex modulation index to link the DC voltage to the real and imaginary parts of the complex AC voltage phasors. The model is based on the transformer-like inverter model introduced in [13] and illustrated in Fig. 1. The electrical schematic includes the LCL filter as well as the VSC losses. The VSC transformer-like model allows to include the converter losses (i.e. the conduction and switching losses) as a voltage source in series with the AC side, and a current source in parallel with the DC side [14] [15]. The DC part is coupled to the AC part using the complex transformer ratio $\overline{M}$ as shown in (9). The transformer ratio represents the reference signal (in the time domain) averaged over one switching period suitably transformed into a phasor representation. In what follows, it is called the *complex modulation index*:

$$\overline{V_2} \quad = \overline{M} V_1, \tag{9}$$

where the overline represents a complex phasor.

The voltages $V_1$ and $\overline{V_2}$ are measured in internal points of the converter, i.e. the terminals of the IGBTs, and are not generally accessible. Therefore, the LCL filter and converter losses need to be included to link the DC voltage at the output of the converter ($V_{dc}$) to the AC voltage at the grid connection ($\overline{V}_{ac}$). The VSC switching and conduction losses are included in the model using their phasor representation as presented in [4]. The AC voltage $\overline{V}_2$ is written as a function of the AC grid voltage and current as:

$$\overline{V}_2 = \overline{V}_{\text{ac}}(1 + \overline{Z}_b\overline{Y}_c) - \overline{I}_{ac}(\overline{Z}_a + \overline{Z}_b + \overline{Z}_a\overline{Z}_b\overline{Y}_c) \tag{10}$$

where $\overline{V}_{\text{ac}}$ is the voltage at the AC node connected to the VSC, $\overline{Z}_a, \overline{Z}_b, \overline{Y}_c$ are the LCL filter parameters as indicated on Fig. 1. The transistor conduction losses are included by a resistive term $R_{eq}$ in $\overline{Z}_b$ as described in [4]. By solving (9) and (10) to $V_{\text{dc}}$, and substituting the current $\overline{I}_{ac}$ using the AC admittance matrix $\overline{I} = \overline{Y}\ \overline{V}$, expression (11) is obtained to relate the DC voltage to the AC voltage phasors in a fully linear way.

$$V_{dc} = C_1 V_j' + C_2 V_l' + C_3 V_j'' + C_4 V_l'', \tag{11}$$

where the subscript $j$ and $l$ refer to the AC branch connected to the VSC, where $j$ is adjacent to the VSC. The real and imaginary parts are indicated using the superscript ' and ".

In the case of unbalanced loading conditions, the AC 3-ph measurements cannot be approximated anymore to only contain the positive sequence and, thus, the measurement

model $\mathbf{H}$ needs to be extended accordingly. Since one DC quantity needs to be related to three complex phasors, the linear VSC model needs to be updated. The complex 3-ph modulation indices $\overline{M}^{abc}$ are transformed into their symmetrical components $\overline{M}^{0pn}$ and expression (9) is rewritten as:

$$\begin{aligned} V_{\text{DC}} =& M_0^{-\prime} V_0' + M_p^{-\prime} V_p' + M_n^{-\prime} V_n' \\ & - \left( M_0^{-\prime\prime} V_0'' + M_p^{-\prime\prime} V_p'' + M_n^{-\prime\prime} V_n'' \right) \end{aligned} \tag{12}$$

By transforming (10) in symmetrical components, and substituting it in (12), a linear expression is obtained to relate the DC voltage to 3-ph AC phasors for unbalanced loading conditions (13). The full mathematical development is presented in [4].

$$\begin{bmatrix} \Re\left((C_1^{0pn} + jC_3^{0pn})^T A^{-1}\right) \\ \Re\left((C_2^{0pn} + jC_4^{0pn})^T A^{-1}\right) \\ \Im\left(-(C_1^{0pn} + jC_3^{0pn})^T A^{-1}\right) \\ \Im\left(-(C_2^{0pn} + jC_4^{0pn})^T A^{-1}\right) \end{bmatrix}^T \begin{bmatrix} V_m'^{abc} \\ V_k'^{abc} \\ V_m''^{abc} \\ V_k''^{abc} \end{bmatrix} = V_{\text{DC}}, \tag{13}$$

The above expression can directly be included in the measurement model as the $[\mathbf{H}_{vsc-ac}\mathbf{H}_{vsc-dc}]$ submatrices.

### C. VSCs complex modulation index

VSCs typically have switching frequencies of tens of kHz. In this experiment, VSCs use symmetric on-time pulse width modulation (PWM) (see Fig. 2), that can be expressed in the Laplace domain as follows:

$$G_{PWM}(j\omega) = cos\left(\frac{\omega D T_s}{2}\right) \angle \left(-\frac{\omega T_s}{2}\right), \tag{14}$$

where $T_s$ is the fixed switching period, $\omega$ the grid frequency and $D$ the duty cycle [16][2]. The magnitude of (14) is close to one, independently of the duty cycle $D$, because of the high switching frequencies that characterise VSCs. Therefore, the modulation process only affects the angle in (14) that has to be compensated for.

The modulation method uses a single or double-updated PWM. The single update is characterized by a computational delay of $T_s$ (as shown in Fig. 2) and a sampling delay of $0.5\ T_s$ is needed to represent the average time for the setpoint implementation. For the double update, the PWM signal is updated twice per switching period and, therefore, characterised by half the delay of the single updated PWM.

Additionally, there is a phase shift caused by the dead time, or blank time ($\delta_{dead}$) , required to prevent the upper and lower transistors of the VSC leg being in *'on'* state simultaneously and causing a short circuit. This blank time causes a phase shift that is dependent on the phase lag of the AC side current with respect to the voltage and it can be modelled as in (16). This is the only phase shift that is non-constant and is function of the state of the network. The dead time causes an offset in voltage at the output of the transistors as illustrated in Fig. 2. The voltage difference between the reference and the observed

[2]Reference [16] gives the Laplace domain formulation for most of the common modulation techniques.

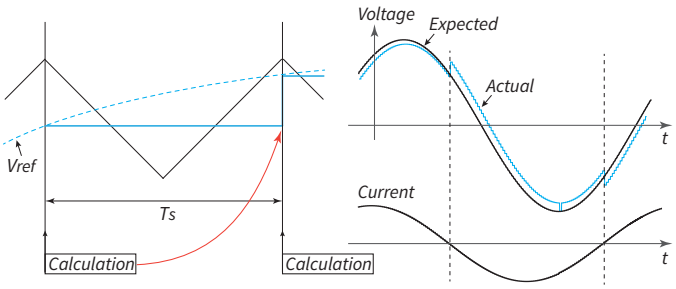


**Fig. 2:** Left: illustration of the single update and symmetric on-time pulse modulation. Right: the influence of the deadtime on the actual voltage reference (obtained in PLECS simulation)

voltage at the IGBT terminals in the time domain can be written as in (15) [17] :

$$v_{ref}(t) - v_2(t) = \begin{cases} 2t_{dead}/T_s v_2(t) & \text{if } i_2(t) > 0 \\ -2t_{dead}/T_s v_2(t) & \text{if } i_2(t) < 0 \end{cases} \tag{15}$$

When computing the Discrete Fourier Transform of this signal, a small different phase angle is obtained compared to the one of the original reference voltage. An analytical expression of the phase shift is experimentally obtained here below to model this phenomenon:

$$\angle\delta_{dead} = 2.5\frac{t_{dead}}{T_s} sin\left(\angle V_2 - \angle I_2\right) \tag{16}$$

Therefore, the true modulation index that represents the AC voltage at the output of the converter ($V_2$) can be written as follows:

$$\overline{M}_{true} = |\overline{M}_{meas.}| \angle \left( \angle \overline{M}_{meas.} - \frac{\omega Ts}{2} - \delta_{update} + \delta_{dead.} \right) \tag{17}$$

### D. DKF Prediction Error Covariance Estimation

A correct assessment of the prediction error covariance matrix $\tilde{\mathbf{P}}_k$ is crucial for the correctness of the DKF. The prediction error covariance is dependent on the process noise $\mathbf{Q}$, which is often hard to assess correctly. Multiple methods have been proposed in the literature for its estimate [18]–[21]. For this experimental validation, the PECE method proposed in [22] is used. This method directly estimates the value of $\tilde{\mathbf{P}}_k$ without needing the assessment of $\mathbf{Q}$. Due to the relatively high computational cost of the PECE, an approximation of the method is implemented. Reference [4] shows that the approximation allows using the PECE method in real-time SE processes with only a limited impact on the state's accuracy. The PECE works as follows: during rapid state changes e.g. a change in the tap position of a transformer, rapid start-up of power electronic converters or load inrushes, the state prediction (3) of the process model is inaccurate. Therefore, the prediction error covariance $\tilde{\mathbf{P}}_k$ estimated by the PECE method inflates to give more weight to the measurements (6). During steady-state operations of the hybrid grid, the opposite happens: the state predictions are more accurate and more weight is given to the process model. Therefore, noise measurements have less influence, so the state estimates will have a lower variance.

**TABLE I:** Data of the installed cables in the hybrid grid.

| Line | R (Ω/km) | X (Ω/km) | B (μS/km) | Amp. (A) | Length (m) |
|---|---|---|---|---|---|
| 1 - 2 | 0.27 | 0.119 | 100.5 | 207 | 70 |
| 2 - 3 | 3.30 | 0.141 | 47.1 | 44 | 30 |
| 2 - 4 | 0.27 | 0.119 | 100.5 | 207 | 35 |
| 4 - 5 | 0.78 | 0.126 | 66.0 | 108 | 30 |
| 4 - 6 | 1.21 | 0.132 | 72.3 | 82 | 105 |
| 6 - 7 | 1.21 | 0.132 | 72.3 | 82 | 30 |
| 4 - 8 | 0.55 | 0.126 | 81.7 | 135 | 70 |
| 8 - 9 | 0.27 | 0.119 | 100.5 | 207 | 30 |
| 8 - 10 | 1.21 | 0.132 | 72.3 | 82 | 105 |
| 10 - 11 | 3.30 | 0.141 | 47.1 | 44 | 30 |
| 10 - 12 | 1.21 | 0.132 | 72.3 | 82 | 35 |
| 12 - 13 | 1.21 | 0.132 | 72.3 | 82 | 30 |
| 7 - 14 | 0.78 | 0.126 | 66.0 | 108 | 38 |
| 9 - 15 | 0.55 | 0.122 | 81.7 | 135 | 114.5 |
| 13 - 16 | 0.55 | 0.122 | 81.7 | 135 | 114.5 |
| 11 - 17 | 0.55 | 0.122 | 81.7 | 135 | 114.5 |
| 7 - 18 | 0.55 | 0.122 | 81.7 | 135 | 114.5 |
| 19 - 23 | 0.075 | 0.089 | 91.7 | 45 | 1000 |
| 20 - 24 | 0.075 | 0.089 | 91.7 | 45 | 1000 |
| 21 - 25 | 0.075 | 0.089 | 91.7 | 45 | 1000 |
| 22 - 26 | 0.075 | 0.089 | 91.7 | 45 | 1000 |

## III. System Architecture

### A. Experimental setup

The SE model described in Section II is validated on the hybrid AC/DC network developed at the EPFL Distributed Electrical Systems Laboratory. The hybrid network consists of an 18-bus AC grid coupled to an 8-bus DC grid using 4 interfacing VSCs. Fig. 3 shows the experimental setup with the AC grid, the DC grid, the interfacing converters and the DMUs. The topology of the hybrid network is shown in Fig. 4. The AC network is a replica of the CIGRE low voltage benchmark grid defined in [23] consisting of real lines (i.e. not emulated) and hosting different distributed energy resources (DERs) such as photovoltaic (PV) plants, a battery energy storage system, an electrical vehicle (EV) charging station and an integrated fuel cell/ electrolyzer system [5]. The three-phase AC grid has a nominal voltage of $400\,\mathrm{V}$ and is connected to the medium voltage grid at node 1. This node serves as the slack bus of the AC microgrid. The DC grid does not host any resources yet, but two DC transformers (DCT) allow the exchange of power between nodes 26 - 23 and 23 - 25. The power flow over the DCTs is proportional to the voltage difference between their input and output [24]. The DC network has a base voltage of $750\,\mathrm{V}$ and consists of 4 line emulators to model lines from $250\,\mathrm{m}$ to $2\,\mathrm{km}$. Table I summarizes the line parameters in the AC and DC networks. The locations of the four AC connection nodes are specifically selected since these nodes are most likely to exhibit grid constraint violations with the connected DER. The VSCs control allows for tracking the reactive power $Q_{ac}$ and the DC voltage $V_{dc}$ setpoint separately. By regulating the DC voltage at the different converter's outputs, the DCTs generate a power flow in the DC grid and active power is injected/absorbed in/from the AC grid (an operational condition that allows to satisfy the grid constraints during high-load conditions). For both networks a base power of $100\,\mathrm{kVA}$ has been chosen.

**TABLE II:** PMU and DMU locations and measurement type in the hybrid AC-DC micro-grid.

| Network | Measurement type | Bus # |
|---|---|---|
| AC | Nodal voltage ($V_{ac}$) | 1,3,5,14 |
| AC | Current injection($I_{ac}$) | 1,3,5,14 |
| AC | Zero injection ($I_{0,ac}$) | 2,4,6,8,10,12 |
| AC | Current flow ($I_{fl,ac}$) | 8-9,10-11,12-13, 9-15,13-16,11-17,7-18 |
| DC | Nodal voltage ($V_{dc}$) | 19,20,21,22,23,24,25,26 |
| DC | Current flow ($V_{dc}$) | 19-23,20-24,21-25,22-26 |
| AFE | Modulation index | AFE 1-4 |

### B. Metering system

The hybrid network is equipped with PMUs and DMUs to provide the SE with high-resolution, time-synchronized measurements. The PMUs are installed in the AC network and measure nodal voltages, current injections and/or current flow phasors. Tab. II summarizes the different measurement types and their location. The location of the measurement devices is also highlighted in Fig. 4. The PMUs are of P-class and extract the phasor of the measured signal's fundamental tone based on the Enhanced Interpolated Discrete Fourier Transform (e-IPDFT) [25]. The data acquisition and the e-IPDFT are implemented on the field programmable gate array of the NI Compact RIO 9063 real-time controller and the communication is implemented on the controller's CPU. The synchrophasor extraction process is time synchronized by GPS. The real-time controller acquires analogue voltages from LEM CV 3-1000 sensors (±0.2% accuracy) and current measurements from LEM LF 205-S sensors (±0.5% accuracy). The PMU complies with the IEEE standard C37.118 [26] with a total vector error of 0.14%. The synchrophasors are encapsulated and streamed every $20\,\mathrm{ms}$ to the PDC using the User Datagram Protocol (UDP) and the IEEE std C37.118.

The DMUs acquire and stream time-synchronized measurements of DC voltages and DC currents using the same procedure as the PMU. Due to the DC nature of the measurements, the e-IpDFT is replaced by an averaging block to average the acquired measurements over the same window as the phasor extraction (i.e., $60\,\mathrm{ms}$). Since no DMU standard exists, the same protocol as for PMUs is used to encapsulate and stream the DC quantities to the PDC. The DMUs are calibrated using the Keysight 3458A digital multimeter over their full operating range to ensure a correct assessment of the measurement noise and to guarantee a zero bias.

### C. Assessment of the measurement noise

The measurement noise defined in (1) needs to be correctly assessed for a proper operation of the SE. The noise originates from both the sensors and inaccuracies in the phasor extraction at the PMU level. The IT instrument class of the sensor satisfies the IEEE standard [27] [28], which defines the ratio limits and angular displacements of the current and voltage transformers. The accuracy of the e-IpDFT PMUs is in the order of $0.1$ % for the magnitude and $10 \times 10^{-3}$ rad for the phase displacement [26]. The noise is assumed to be white and uncorrelated with the instrument transformers' noise.

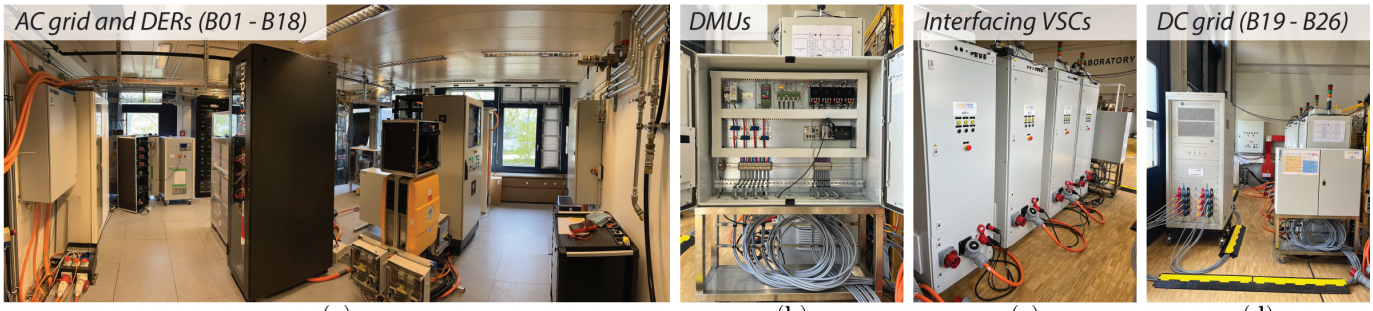


**Fig. 3:** The experimental setup: **(a)** AC grid and DERs ($B01 - B18$), **(b)** DC measurement units ($DMU\ 1 - 8$), **(c)** interfacing VSCs ($VSC\ 1 - 4$) and **(d)** DC grid ($B19 - B26$).

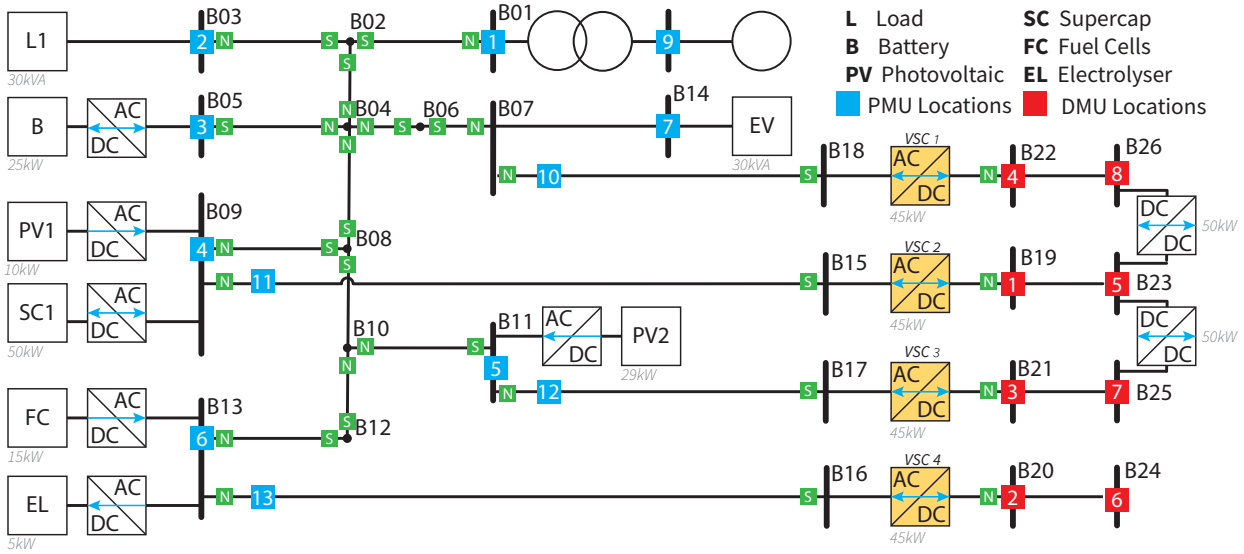


**Fig. 4:** Hybrid AC/DC microgrid developed at the EPFL: topology and DERs power ratings.

Therefore, following the hypothesis for the summation of uncorrelated normal distributions, the cumulative maximum errors of the sensors and the PMUs are computed by adding the corresponding magnitude and phase errors. The cumulative standard deviation of the measurement noise is equal to one-third of the maximum errors. Since the phasors are expressed in Cartesian coordinates, the measurement noise also needs to be transformed to this coordinate base. Reference [29] defines the coordinate transformation and shows it does not influence the normality or bias of the noise noticeably.

Using the Keysight digital multimeter, the measurement noise of the sensors and DMU are quantified precisely. The measurements have a standard deviation of around $8.7 \times 10^{-6}$ p.u. for the voltage and $2.3 \times 10^{-5}$ p.u. for the current.

### *D. Supervisory Control and Data acquisition*

The SCADA system consists of the PDC and the SE stages. The SCADA system is implemented in the Labview programming environment on a dedicated Windows machine [5]. The machine is time-synchronised by the Tekron TTM 01-G GPS clock.

The **PDC** collects the UDP packages coming from the PMUs and DMUs and mitigates the latency variations introduced by the different components in the network [26]. The data aggregation and time alignment are achieved using a fixed-size circular buffer [30]. The buffer is implemented as a 2D array with N rows, for each stored timestamp, and as many columns as PMU and DMU measurements. The number of rows equals the buffer depth and thus the number of time stamps stored. When the first row is full, meaning each measurement of the first timestamp has arrived or when the waiting time is over, the data in this row is pushed to the SE. The SE deals with possible missing data that did not arrive in time or that went lost in the telecommunication network. The missing data is replaced with pseudo measurements computed using the previously estimated state [31]. This architecture allows for a minimal PDC latency while still having robustness for data incompleteness [30].

The **SE** algorithm is based on the DKF presented in Section II and implemented in the same Labview environment. The full structure of the measurement model, measurement and state vector for the hybrid AC/DC grid is given in (18). The 116 state variables of the hybrid network are the nodal real and imaginary 3-ph AC and real DC voltages. The measurements are provided by the PMUs and DMUs along with the zero injection nodes constraints ($I_{0,ac}$) and the VSC equations (13). The system counts 170 unique measurements and has a redundancy factor of 1.47. Furthermore, the measurement

locations and types are chosen to insure the observability criteria is satisfied at all time (i.e., it is full rank).

$$\begin{bmatrix} V'_{\text{ac}} \\ V'_{\text{ac*}} \\ V''_{\text{ac}} \\ V''_{\text{ac*}} \\ I'_{\text{ac}} \\ I''_{\text{ac}} \\ I'_{0,\text{ac}} \\ I''_{0,\text{ac}} \\ I'_{\text{fl,ac}} \\ I''_{\text{fl,ac}} \\ V_{\text{dc}} \\ V_{\text{dc*}} \\ I_{\text{dc}} \\ I_{\text{dc*}} \\ \hat{A}\hat{F}\hat{E} \end{bmatrix} = \left[\begin{array}{ccccccc} \mathbf{I} & & & & & & \\ & \mathbf{I} & & & & & \\ & & \mathbf{I} & & & & \\ & & & \mathbf{I} & & & \\ \mathbf{G}_{\text{ac}} & & -\mathbf{B}_{\text{ac}} & & & & \\ \mathbf{B}_{\text{ac}} & & \mathbf{G}_{\text{ac}} & & & & \\ \mathbf{G}_{\text{ac}} & & -\mathbf{B}_{\text{ac}} & & & & \\ \mathbf{B}_{\text{ac}} & & \mathbf{G}_{\text{ac}} & & & & \\ & \mathbf{g}_{\text{ac}} & & -\mathbf{b}_{\text{ac}} & & & \\ & \mathbf{b}_{\text{ac}} & & \mathbf{g}_{\text{ac}} & & & \\ & & & & \mathbf{I} & & \\ & & & & & \mathbf{I} & \\ & & & & \mathbf{G}_{\text{dc}} & \mathbf{G}_{\text{dc}} & \\ & & & & \mathbf{G}_{\text{dc}} & \mathbf{G}_{\text{dc}} & \\ \mathbf{C_1} & \mathbf{C_2} & \mathbf{C_3} & \mathbf{C_4} & -\mathbf{I} & & \end{array}\right] \begin{bmatrix} V'_{\text{ac}} \\ V'_{\text{ac*}} \\ V''_{\text{ac}} \\ V''_{\text{ac*}} \\ V_{\text{dc}} \\ V_{\text{dc*}} \end{bmatrix} \tag{18}$$

The **adaptive KF** estimates the prediction error covariance and is implemented in a sequential way as in the original DKF architecture. Since the PECE method directly computes $\tilde{\mathbf{P}}$, it replaces equation (4) of the DKF. We can observe that the SE computation time could be further improved by running the PECE method in parallel on a dedicated CPU core. However, as will be shown in the next section, the computation time of the PECE algorithm is around $150\,\text{ms}$ and is thus already suitable for a real-time SE.

## IV. Results and Discussion

### A. Measurement Residual Noise Hypothesis Validation

Since in a real-world experiment the true states are unobservable, the prediction and estimation noise hypothesis verification method used in [4] cannot be adopted here. Therefore, the validation is based on the analysis of the measurement residuals, i.e. the difference between the measurements and the reconstructed measurements computed using the estimated states: $\boldsymbol{r} = \boldsymbol{z} - \boldsymbol{H}\hat{\boldsymbol{x}}$. Only when no bad data is present, this metric can be used to validate the measurement model. Intuitively this can be explained as follows: when no bad data is present, the measurements are unbiased and the distributions are within the measurement noise model and the linear measurement model is an exact mapping between the measurements and the estimated states. Therefore, if the residuals are zero-biased and have a distribution that is smaller than the three-sigma limit of the theoretical distribution, the measurement model is correct. The theoretical covariance matrix of the residuals of the DKF is presented in [4] and can be computed as:

$$\mathbf{T} = \mathbf{R}(\mathbf{H}\tilde{\mathbf{P}}\mathbf{H}^{\intercal})^{-1}\mathbf{R}. \tag{19}$$

The experiment has been conducted on December 9, 2022, in the afternoon during a quasi-steady-state operation of the network. Tab. III shows the setpoints and loading conditions of the operational resources. The voltage difference between converter 1 and 2 generates an active power flow of around $10\,\text{kW}$. The controllable load connected in Bus 3 creates an unbalanced loading condition by absorbing power only in phase c.

**TABLE III:** PMU and DMU locations and measurement types.

| Resouce | Setpoints | Resource | Setpoints |
|---|---|---|---|
| AFE 1 | $-10\,\text{kVAr}$, $741\,\text{V}$ | PV 1 | $\sim 4\,\text{kW}$ |
| AFE 2 | $5\,\text{kVAr}$, $750\,\text{V}$ | PV 2 | $\sim 6\,\text{kW}$ |
| AFE 3 | $-15\,\text{kVAr}$, $750\,\text{V}$ | Load | $6.32\,\text{kW}$,$1.5\,\text{kVAr}$ (ph-c) |
| AFE 4 | $5\,\text{kVAr}$, $750\,\text{V}$ | EV | $0\,\text{kW}$ |

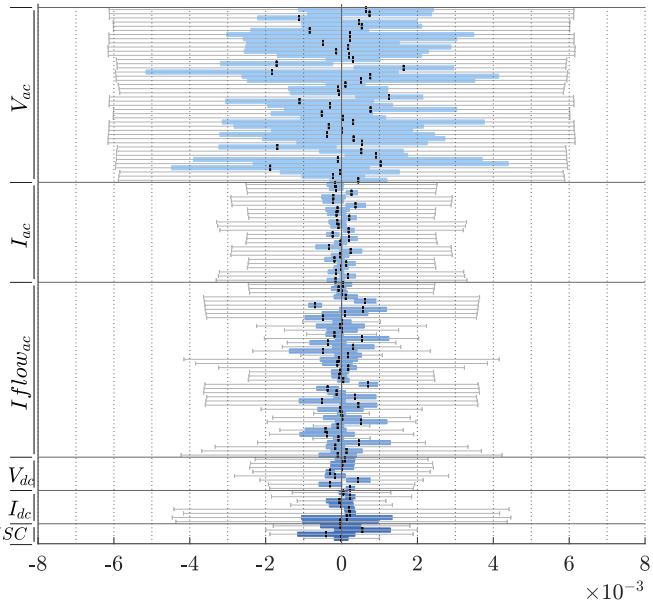


**Fig. 5:** Distribution of all the measurement residuals for the DKF method (in p.u.)

Fig. 5 shows the distribution of every measurement residual. The type of measurements (AC or DC voltages or currents) is indicated on the left vertical axis. The mean and the standard deviation of all the residuals are displayed by the blue bars and the three-sigma limits of the expected distribution are shown by the grey error bars. The distributions are computed over a $10\,\text{min}$ horizon and are all shown in p.u.

We can see that the residuals have a mean that is very close to zero and a standard deviation that is well below the three $\sigma$ limit of the expected distribution. This confirms the correctness of the measurement model and thus the SE of the hybrid AC/DC microgrid [3].

[3]Notice that the distribution of the AC current residuals is much smaller than the one of the AC voltages. The reason for this is the low loading condition of the grid: the measured voltages are typically 1 p.u. and have an accuracy of 0.2%. The currents, on the other hand, are around 0.1 p.u. with an accuracy of 0.5%. Therefore, in absolute value, the measurement error of the currents will be much smaller and this has a direct impact on the residuals. Furthermore, the DC residuals have a small distribution because of the very low DC measurement noise.

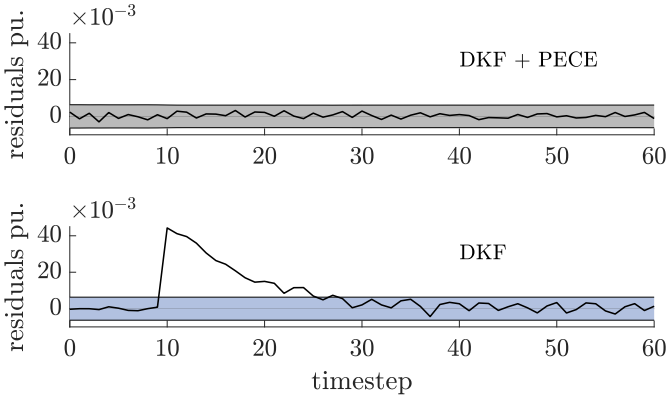


**Fig. 6:** Comparison of the dynamic response between the DKF and the Adaptive KF based on the PECE method

### *B. Performance of the PECE method*

The performance of the PECE method is assessed in a dedicated experiment where the hybrid grid states vary over time. The initial hybrid grid is in quasi-steady-state conditions and a step is introduced in the setpoint of VSC 4 where the reactive power output is suddenly increased from $5\,\mathrm{kVAr}$ to $15\,\mathrm{kVAr}$ (an increase of $0.1$ p.u.). The residuals of the voltage measurements of phase a in bus 5 are shown over time in Fig. 6 and the $3\sigma$ boundaries of the expected residual variance are indicated in the shaded area. We see that, during the step, the residuals of the DKF SE increase strongly and exceed the $3\sigma$ limits. In DKF coupled with the PECE method, however, the residuals do not exceed the bounds because the PECE method responds instantaneously to the step. This directly affects the accuracy of the estimated state. Notice here that we cannot determine the accuracy of the SE since the 'true' state cannot be observed in a real-world experiment. Additionally, we can also observe that, before and after the step, the variation of the residuals is significantly lower for the PECE method. This is because the prediction covariance noise is estimated at every timestep, therefore both in steady-state conditions and during dynamics, the PECE method will have superior performance.

### *C. Time Latency Analysis*

The time latency for the different elements in the SE process, i.e. the phasor extraction, the telecommunication network, and the time-alignment of the PDC and the SE process, is analysed. The measurement devices, PDC and SE computer are all time-synchronised by means of the UTC-GPS and, thus, the latency of each element can be assessed individually as a cumulative distribution function as shown in Fig. 7. The time latency analysis is shown for both the normal DKF and the DKF coupled with the PECE where we can see that the latter is around $150\,\mathrm{ms}$ longer due to the computation of the process noise covariance matrix. We can observe that the maximum latencies of the DKF with the PECE method are below $400\,\mathrm{ms}$, thus compatible with real-time controls.

## V. CONCLUSION

In this paper, we presented the experimental validation of the novel SE process for hybrid AC/DC microgrids proposed in the authors' previous work. The electrical hybrid network

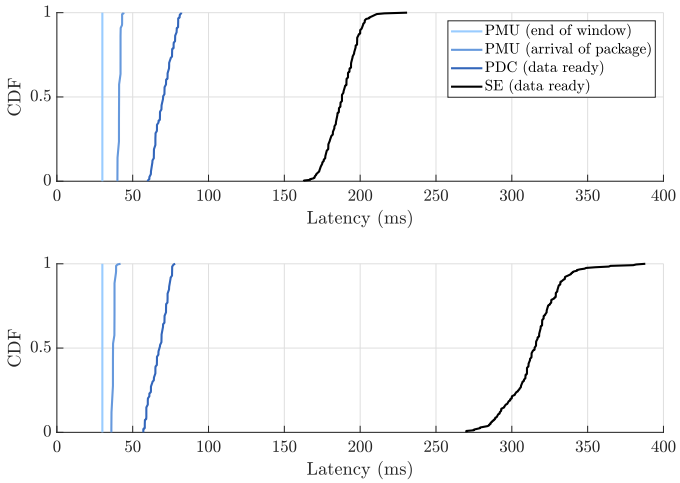


**Fig. 7:** Cumulative distributions of the time latencies of the individual sub-processes of the SE process. Top: for the DKF. Bottom: for the approximated PECE diag method ,(DKF+PECE)

developed at the EPFL consists of a DC network that is interconnected with the AC grid in four nodes using VSCs. Time synchronised measurement devices (i.e. PMUs in the AC system and DMUs in the DC system) provide low latency measurements at a rate of tens of estimates per second. The PDC receives the measurements, time-aligns them and streams them to the SE process relying on the unified and linear measurement model.

Because of the unobservability of the network's true state, the performance of the SE process is analysed using the hypothesis verification on the measurement residuals. It is shown that the residuals are zero-biased and have a variance well below the three-sigma value of the theoretical distribution and therefore the SE is validated. To cope with frequent step changes in microgrids, an adaptive SE based on the PECE method is implemented. We show that the PECE method reliably tracks the system's state during severe step change dynamics and during steady-state operation of the hybrid microgrid. Finally, the time latency of both SE methods, the DKF and the DKF coupled with the PECE method, is presented demonstrating the compatibility of the latter with real-time control needs.

## REFERENCES

[1] N. Eghtedarpour and E. Farjah, "Power control and management in a hybrid ac/dc microgrid," *IEEE Transactions on Smart Grid*, vol. 5, no. 3, pp. 1494–1505, 2014.

[2] Y. R. Li, F. Nejabatkhah, and H. Tian, *Smart Hybrid AC/DC Microgrids*, 2023, pp. 1–20.

[3] R. Gupta, F. Sossan, and M. Paolone, "Grid-aware distributed model predictive control of heterogeneous resources in a distribution network: Theory and experimental validation," *IEEE Transactions on Energy Conversion*, vol. 36, no. 2, pp. 1392–1402, 2020.

[4] W. Lambrichts and M. Paolone, "Linear recursive state estimation of hybrid and unbalanced ac/dc micro-grids using synchronized measurements," *IEEE Transactions on Smart Grid*, 2022.

[5] L. Zanni, "Power-system state estimation based on pmus static and dynamic approaches - from theory to real implementation," Ph.D. dissertation, EPFL, Lausanne, 2017. [Online]. Available: http://infoscience.epfl.ch/record/228451

[6] N. Xia, H. B. Gooi, S. Chen, and W. Hu, "Decentralized state estimation for hybrid ac/dc microgrids," *IEEE Systems Journal*, vol. 12, no. 1, pp. 434–443, 2016.

[7] X. Kong, Z. Yan, R. Guo, X. Xu, and C. Fang, "Three-stage distributed state estimation for ac-dc hybrid distribution network under mixed measurement environment," *IEEE Access*, vol. 6, pp. 39 027–39 036, 2018.

[8] Z. Fang, Y. Lin, S. Song, C. Li, X. Lin, F. Wang, and Y. Lu, "A comprehensive framework for robust ac/dc grid state estimation against measurement and control input errors," *IEEE Transactions on Power Systems*, 2021.

[9] W. Li, L. Vanfretti, and J. H. Chow, "Pseudo-dynamic network modeling for pmu-based state estimation of hybrid ac/dc grids," *IEEE Access*, vol. 6, pp. 4006–4016, 2017.

[10] M. Ayiad, H. Leite, and H. Martins, "State estimation for hybrid vsc based hvdc/ac transmission networks," *Energies*, vol. 13, no. 18, p. 4932, 2020.

[11] A. Abur and A. G. Exposito, *Power system state estimation: theory and implementation*. CRC press, 2004.

[12] A. S. Debs and R. E. Larson, "A dynamic estimator for tracking the state of a power system," *IEEE Transactions on Power Apparatus and Systems*, no. 7, pp. 1670–1678, 1970.

[13] F. Scapino, "A transformer-like model for the dc/ac converter," in *IEEE International Conference on Industrial Technology, 2003*, vol. 1. IEEE, 2003, pp. 625–630.

[14] A. Fratta and F. Scapino, "Modeling inverter losses for circuit simulation," in *2004 IEEE 35th Annual Power Electronics Specialists Conference*, vol. 6. IEEE, 2004, pp. 4479–4485.

[15] F. Scapino , "Vsi lossy models for circuit simulation including high-impedance state," in *Proceedings of the IEEE International Symposium on Industrial Electronics, 2005.*, vol. 2, 2005, pp. 565–570 vol. 2.

[16] D. M. Van de Sype, K. De Gussemé, A. P. Van den Bossche, and J. A. Melkebeek, "Small-signal laplace-domain analysis of uniformly-sampled pulse-width modulators," in *2004 IEEE 35th Annual Power Electronics Specialists Conference (IEEE Cat. No. 04CH37551)*, vol. 6. IEEE, 2004, pp. 4292–4298.

[17] M. N. Undeland, W. P. Robbins, and N. Mohan, "Power electronics," *Converters, Applications, and Design*, 1995.

[18] B. J. Odelson, M. R. Rajamani, and J. B. Rawlings, "A new autocovariance least-squares method for estimating noise covariances," *Automatica*, vol. 42, no. 2, pp. 303–308, 2006.

[19] L. Zanni, S. Sarri, M. Pignati, R. Cherkaoui, and M. Paolone, "Probabilistic assessment of the process-noise covariance matrix of discrete kalman filter state estimation of active distribution networks," in *2014 International Conference on Probabilistic Methods Applied to Power Systems (PMAPS)*. IEEE, 2014, pp. 1–6.

[20] G. Noriega and S. Pasupathy, "Adaptive estimation of noise covariance matrices in real-time preprocessing of geophysical data," *IEEE transactions on geoscience and remote sensing*, vol. 35, no. 5, pp. 1146–1159, 1997.

[21] K. Myers and B. Tapley, "Adaptive sequential estimation with unknown noise statistics," *IEEE Transactions on Automatic Control*, vol. 21, no. 4, pp. 520–523, 1976.

[22] L. Zanni, J.-Y. Le Boudec, R. Cherkaoui, and M. Paolone, "A prediction-error covariance estimator for adaptive kalman filtering in step-varying processes: Application to power-system state estimation," *IEEE Transactions on Control Systems Technology*, vol. 25, no. 5, pp. 1683–1697, 2016.

[23] S. Barsali, K. Strunz, and Z. Styczynski, "Cigre' task force c6.04.02: Developing benchmark models for integrating distributed energy resources," in *2006 IEEE Power Engineering Society General Meeting*, 2005.

[24] R. P. Barcelos, J. Kucka, and D. Dujic, "Power reversal algorithm for resonant direct current transformers for dc networks," *IEEE Access*, vol. 10, pp. 127 117–127 127, 2022.

[25] P. Romano, "Dft-based synchrophasor estimation algorithms and their integration in advanced phasor measurement units for the real-time monitoring of active distribution networks," EPFL, Tech. Rep., 2016.

[26] "Ieee standard for synchrophasor measurements for power systems," *IEEE Std C37.118.1-2011*, pp. 1–61, 2011.

[27] "Instrument transformers:, "additional requirements for electronic current transformers,"," Standard IEC, Tech. Rep. 61869-2, 2011.

[28] "Instrument transformers:, "additional requirements for electronic current transformers,"," Standard IEC, Tech. Rep. 61869-3, 2011.

[29] M. Paolone, J.-Y. Le Boudec, S. Sarri, and L. Zanni, "Static and recursive pmu-based state estimation processes for transmission and distribution power grids," The Institution of Engineering and Technology-IET, Tech. Rep., 2015.

[30] A. Derviškadić, P. Romano, M. Pignati, and M. Paolone, "Architecture and experimental validation of a low-latency phasor data concentrator," *IEEE Transactions on Smart Grid*, vol. 9, no. 4, pp. 2885–2893, 2018.

[31] M. Pignati, L. Zanni, S. Sarri, R. Cherkaoui, J.-Y. Le Boudec, and M. Paolone, "A pre-estimation filtering process of bad data for linear power systems state estimators using pmus," in *2014 Power Systems Computation Conference*. IEEE, 2014, pp. 1–8.